Physiologic Diversity and Development of Intrinsically Photosensitive Retinal Ganglion Cells

ARTICLE *in* NEURON · JANUARY 2006

Impact Factor: 15.05 · DOI: 10.1016/j.neuron.2005.09.031 · Source: PubMed

Neuron, Vol. 48, 987–999, December 22, 2005, Copyright ©2005 by Elsevier Inc. DOI 10.1016/j.neuron.2005.09.031

Physiologic Diversity and Development of Intrinsically Photosensitive Retinal Ganglion Cells

Daniel C. Tu,[1,6] Dongyang Zhang,[1,6] Jay Demas,[2] Elon B. Slutsky,[4] Ignacio Provencio,[4,5] Timothy E. Holy,[2] and Russell N. Van Gelder[1,3,*]
[1] Department of Ophthalmology and Visual Sciences
[2] Department of Anatomy and Neurobiology
[3] Department of Molecular Biology and Pharmacology
Washington University Medical School
St. Louis, Missouri 63110
[4] Department of Anatomy,
Physiology, and Genetics and
The Circadian Research Center
Uniformed Services University
Bethesda, Maryland 20814
[5] Department of Biology
University of Virginia
Charlottesville, Virginia 22903

Summary

Intrinsically photosensitive retinal ganglion cells (ipRGCs) mediate numerous nonvisual phenomena, including entrainment of the circadian clock to light-dark cycles, pupillary light responsiveness, and light-regulated hormone release. We have applied multielectrode array recording to characterize murine ipRGCs. We find that all ipRGC photosensitivity is melanopsin dependent. At least three populations of ipRGCs are present in the postnatal day 8 (P8) murine retina: slow onset, sensitive, fast off (type I); slow onset, insensitive, slow off (type II); and rapid onset, sensitive, very slow off (type III). Recordings from adult *rd/rd* retinas reveal cells comparable to postnatal types II and III. Recordings from early postnatal retinas demonstrate intrinsic light responses from P0. Early light responses are transient and insensitive but by P6 show increased photosensitivity and persistence. These results demonstrate that ipRGCs are the first light-sensitive cells in the retina and suggest previously unappreciated diversity in this cell population.

Introduction

Mice blind from loss of rod and cone function retain light-dependent entrainment of the circadian clock to light-dark cycles, pupillary light responsiveness, and light-dependent suppression of nocturnal melatonin release (Freedman et al., 1999; Lucas et al., 1999, 2001). These responses are mediated by a class of retinal ganglion cells that are intrinsically photosensitive (ipRGCs), which comprise 1%–2% of all ganglion cells (Berson et al., 2002; Hattar et al., 2002). In the mouse, these cells appear to project exclusively to nonvisual regions of the central nervous system, including the suprachiasmatic nuclei (SCN; site of the behavioral circadian pacemaker) and the olivary pretectum (OPN; initiator of the pupillary light response) (Hattar et al., 2002). ipRGCs utilize the novel opsin melanopsin as their photopigment (Hannibal et al., 2002; Hattar et al., 2003; Panda et al., 2003; Provencio et al., 1998, 2000, 2002b).

To date, physiological characterization of ipRGCs has relied primarily on their identification by retrograde transport of fluorescent dyes from animals stereotactically injected in the SCN or OPN, followed by patch-clamp recording of individual cells (Berson et al., 2002; Dacey et al., 2005). However, this technique has significant limitations, principally the small numbers of cells that can be studied from an individual animal, the inability to study animals where stereotaxic injection is problematic (such as immature animals), and the difficulty in studying cell-cell coupling among ipRGCs. Calcium dye imaging of ipRGCs has been employed to circumvent these problems (Sekaran et al., 2003, 2005); however, it is unclear at present to what extent changes in calcium flux reflect cell firing in ipRGCs.

The early development of ipRGCs is particularly intriguing, as recent studies have suggested that the mammalian inner retina expresses melanopsin before birth (Fahrenkrug et al., 2004) and is light responsive from birth (Hannibal and Fahrenkrug, 2004; Sekaran et al., 2005). However, these studies have not been able to characterize the physiological output (action potentials) of young ipRGCs. Visual signaling is not thought to develop until eye opening (~postnatal day 10 [P10]), based on morphologic (Ratto et al., 1991) or electroretinographic (Bakall et al., 2003) evidence; thus, if ipRGCs are photosensitive and capable of signaling from birth, these would be the first photosensitive cells in the retina and their firing the first light-dependent signaling to the brain.

To further characterize inner retinal photoresponses, we have applied multielectrode array (MEA) recording techniques (Meister et al., 1994; Wong et al., 1993) to study populations of ipRGCs ex vivo from intact retinas. These recordings provide data confirming that all inner retinal light responses of postnatal mice are dependent on the nonvisual photopigment melanopsin. These recordings also reveal previously unappreciated physiologic diversity among ipRGCs. Additionally, we demonstrate that ipRGCs are light responsive and capable of triggering action potentials from birth but show remarkable physiologic and anatomic changes during early postnatal development.

Results

Establishment of Conditions for Isolation of Melanopsin-Dependent ipRGC Signals on MEA

To simultaneously examine multiple ipRGC light responses from an individual retina, we placed a P8 retina ganglion cell-side down on a planar MEA with a grid of 60 recording electrodes (30 μm diameter) placed 200 μm apart. At this developmental age, outer retinal photoreception does not yet contribute to ganglion cell light responses; however, the inner retina does participate in spontaneous waves of activity (Wong et al., 1993). To

*Correspondence: vangelder@vision.wustl.edu
[6] These authors contributed equally to this work.

block this activity, which obscures ipRGC responses and induces refractory behavior in these cells, we performed recordings in a drug cocktail with glutamatergic and cholinergic inhibitors (see Experimental Procedures). Figure 1A shows a recording from a single MEA electrode, monitoring light-induced action potentials from an individual ipRGC. Spike sorting algorithms were employed to isolate single units from electrodes recording multiple waveforms (Holy et al., 2000), allowing routine isolation of >20 light-responsive single units per retina.

While we observed three distinct types of ipRGCs in P8 retina (see below), most ipRGCs (70%–75%) had physiology comparable to that previously described (Berson et al., 2002). Under saturating or near-saturating light stimulation, these ipRGCs initiated spike trains with a delay of a few seconds following light onset (Figures 1A and 1B). Activity rapidly reached a peak firing rate before settling to a steady-state firing rate that was ~50% of peak rate. Precision of single-cell responses to identical stimuli was remarkable (Figure 1C); total spike counts during successive 1 min stimuli with narrow band-pass filtered light typically varied by ≤2%. Following lights off, activity decreased to baseline dark levels over ~5–30 s.

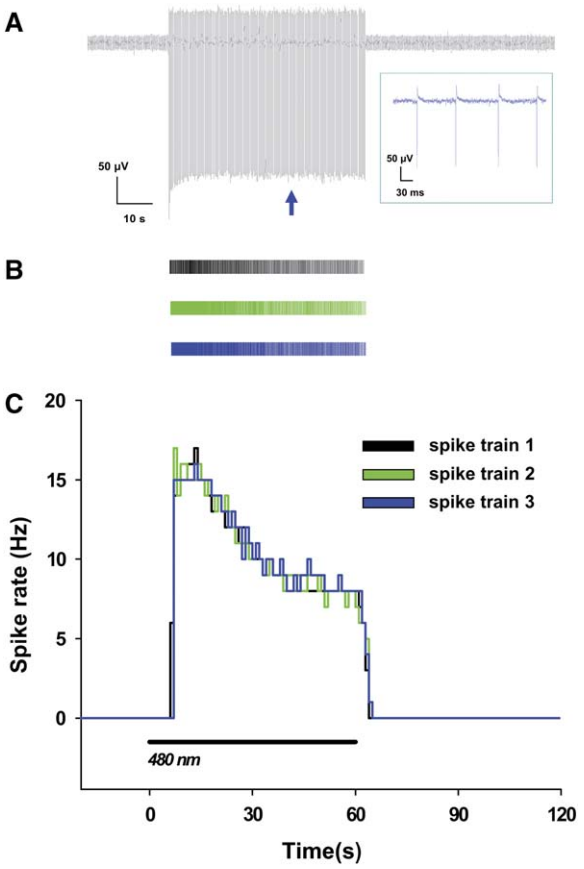

Figure 1. MEA Recording of ipRGC Light Responses

Shown is a recording from a single MEA electrode, monitoring an intrinsically photosensitive cell from a P8 retina, stimulated by three consecutive identical light pulses (480 nm, 1.13×10^{13} photons·cm^{-2}·s^{-1}, 60 s, represented on bar below image) separated by 3 min of darkness. (A) Extracellular recording of action potentials in response to the second light pulse. Inset shows magnification of recording at arrow. (B) Spike trains in response to each of the three light pulses plotted on separate rows. (C) Time series of firing rates of the cell shown in (A) and (B) during the three identical stimuli (1 s bins). Retina was superperfused with solutions containing glutamatergic and cholinergic inhibitors (see Experimental Procedures).

Intrinsic Inner Retinal Photosensitivity Is Melanopsin Dependent

To determine whether the photopigment melanopsin is required for all observed postnatal inner retinal light responses, we compared the inner retinal activity of P8 melanopsin-deficient (*opn4*$^{-/-}$) and wild-type mice in response to light and extracellular KCl perfusion. While both genotypes showed equal action potential firing in response to high-KCl bath, only wild-type retinas showed light-responsive activity (Figure 2B). Out of 180 electrodes from three wild-type P8 retinas from three different animals, 173 electrodes recorded KCl-responsive action potentials, 153 of which also recorded light-responsive activity (see Experimental Procedures). Conversely, in measurements of 300 electrodes recorded from five P8 *opn4*$^{-/-}$ retinas from five different mice, 281 electrodes showed KCl-responsive spikes, while none exhibited light-induced activity. Indeed, in recordings from retinas from 12 individual *opn4*$^{-/-}$ mice of different ages (P4–P10), we saw no light-dependent inner retinal signals. These results are consistent with previous, smaller surveys of potential ipRGCs in *opn4*$^{-/-}$ retinas (Lucas et al., 2003) and strongly suggest that all inner retinal photoreception is melanopsin dependent.

MEA Recordings Reveal Three Classes of ipRGCs in the P8 Retina

Examination of P8 ipRGCs using the MEA recording technique revealed three patterns of light-responsive activity: (1) long latency to activity onset at subsaturating irradiance, high photosensitivity, and fast termination of activity following lights off (Figures 3A and 3B); (2) long latency to activity onset at subsaturating irradiance, low photosensitivity, and slow termination of activity following lights off (Figures 3C and 3D); (3) short latency to activity onset at subsaturating irradiance, high photosensitivity, and very slow termination of activity following lights off (Figures 3E and 3F). Table S1 in the Supplemental Data available with this article online summarizes characteristics of the different types of ipRGC responses observed in P8 retinas.

We found that the different types of postnatal ipRGC responses, categorized initially by a human observer, could be impartially distinguished on the basis of quantitative measurements of kinetics and photosensitivity. To segregate response types, we first examined the latency to activity onset in response to 1.10×10^{12} photons·cm^{-2}·s^{-1} 480 nm light; cells with a very short latency to activity onset (<12 s) were categorized as postnatal type III cells (Figure 3G). The remaining cells were labeled postnatal type I or type II by examining their sensitivity to 480 nm light (Figure 3H). To quantify photosensitivity, irradiance-response curves were generated for each individual cell (with total number of light-induced action potentials utilized as the response parameter); the sensitivity of each cell to 480 nm light

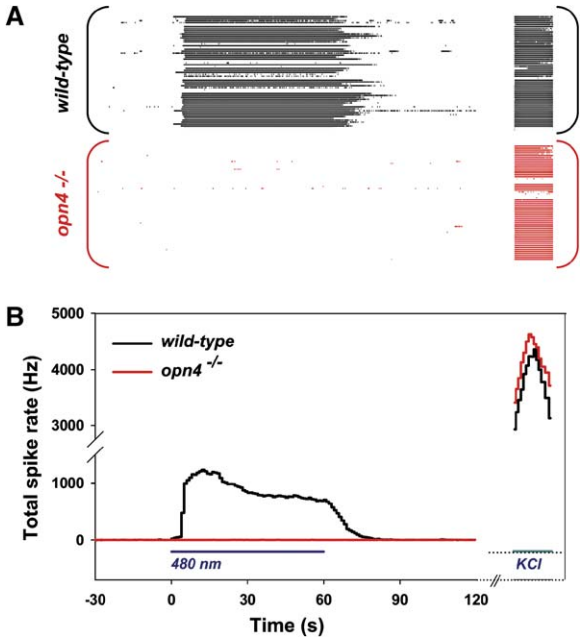

Figure 2. Melanopsin Is Required for Intrinsic Photosensitivity of Postnatal Mouse Inner Retinal Cells

(A) Spike times of action potentials recorded from P8 C57Bl/6 wild-type (black) and P8 *opn4*$^{-/-}$ (red) retinas in response to light (left, 480 nm, 60 s, 5.0 × 10^{13} photons·cm^{-2}·s^{-1}, see bar below) and during high-K^+ bath perfusion (right, see bar below).

(B) Action potentials from the 60 electrodes shown in (A) were summed and plotted as a histogram with 1 s bins. All experiments were performed on retinas superperfused with solutions containing glutamatergic and cholinergic inhibitors (see Experimental Procedures).

was calculated as the irradiance yielding half-maximal response (log IR50) (see Experimental Procedures). More sensitive cells (log IR50 < 12.85) were categorized as postnatal type I, while less sensitive cells (log IR50 > 12.85) were labeled as postnatal type II. These latency and sensitivity parameters divided postnatal ipRGC light responses into distinct populations (Figures 3G and 3H).

Among a sample of 254 P8 ipRGCs, we observed 72% type I, 15% type II, and 13% type III cells. A survey of spike amplitudes among cell types revealed that postnatal type III ipRGCs have significantly smaller action potential amplitudes than the other types (postnatal type I = −71.8 ± 8.6 μV [mean ± SEM], n = 55; type II = −59.67 ± 8.8 μV, n = 16; type III = −28.9 ± 3.7 μV, n = 17; p = 0.0015 by ANOVA, with postnatal type III significantly different than type I or II by post hoc testing [p < 0.05]). Because there is a selection bias against recording and isolating small amplitude action potentials, it is possible that postnatal type III cells may be underrepresented in our analyzed population of P8 ipRGCs.

Average irradiance-response curves to 480 nm light were generated for each cell type (Figure 3I; also see Figure S1). Postnatal type II cells showed an ~10-fold decrease in sensitivity compared with type I and type III cells. Interestingly, postnatal type III cells typically had irradiance-response relationships that were more shallow in slope than those of either postnatal type I or type II cells.

The spectral sensitivity of inner retinal photoreception in mice has been inferred by measurements of the action spectra for nonvisual behaviors, including circadian phase shifting (Hattar et al., 2003) and pupillary light responses in mice lacking outer retinal photoreceptors (Lucas et al., 2001). Both behaviorally measured spectra are similar, with an excellent fit to an opsin pigment template with peak sensitivity of ~480 nm. A similar spectrum for ipRGC spectral sensitivity has been determined based on patch-clamp recording of ipRGCs in rats (Berson et al., 2002) and macaque monkeys (Dacey et al., 2005) and has been seen for melanopsin-dependent photosensitivity in at least some cell culture-based heterologous expression systems (Panda et al., 2005; Qiu et al., 2005; although see Melyan et al., 2005; Newman et al., 2003 for exceptions). We determined the action spectrum for postnatal P8 type I ipRGCs (n = 100) by analyzing responses to 1 min pulses of narrow bandpass filtered light of different wavelengths. Irradiance-response curves generated for each wavelength tested appeared univariant, suggesting a single photopigment (Figure S2). Irradiance-response curves were used to calculate log relative spectral sensitivities, which were then fit with an opsin template (see Experimental Procedures) yielding an action spectrum with peak at 481.0 ± 1.6 nm (Figure 3J), in excellent agreement with previously described melanopsin-based action spectra. Action spectra for postnatal type II (n = 22) and type III cells (n = 14) (Figure 3J) were fit with the same template and had a similar peak wavelength as postnatal type I cells, suggesting a common photopigment for all three cell types. λ_{max} for postnatal type II cells was found to be 480.0 ± 3.7 nm; λ_{max} for postnatal type III cells was found to be 479.5 ± 2.3 nm.

Physiologic Diversity in Adult *rd/rd* Retinas

Much of the physiology of nonvisual photoreception has been determined in the *rd/rd* retinal degenerate mouse (Foster et al., 1991; Panda et al., 2003; Van Gelder et al., 2003). The absence of rods and most cones in the adult *rd/rd* mouse makes it particularly amenable to recording ipRGC responses. To isolate adult *rd/rd* mouse ipRGC light responses (and most accurately compare these to the responses of postnatal ipRGCs), we performed recordings with the same glutamatergic and cholinergic inhibitors used to describe postnatal ipRGCs (see Experimental Procedures). These conditions blocked all signaling from residual outer retinal photoreceptors, allowing us to isolate and record well-defined ipRGC light responses from adult mice (Figure S3).

Analysis of 48 ipRGCs recorded from four adult *rd/rd* retinas showed substantial physiologic diversity in ipRGC physiology. We could appreciate two patterns of activity, which corresponded roughly to two of the three types seen in postnatal retinas (Table S1). Because of similarities to postnatal type II and III cells, we have termed the adult groups adult type II and type III, respectively. Adult type II cells showed a long latency to activity onset (especially at subsaturating irradiance) and slow termination of activity following lights off (Figures 4A and 4B). In contrast, adult type III cells showed very short latency to activity onset (even in response to dim subsaturating irradiance) and highly sustained activity after lights off, comparable to postnatal type III

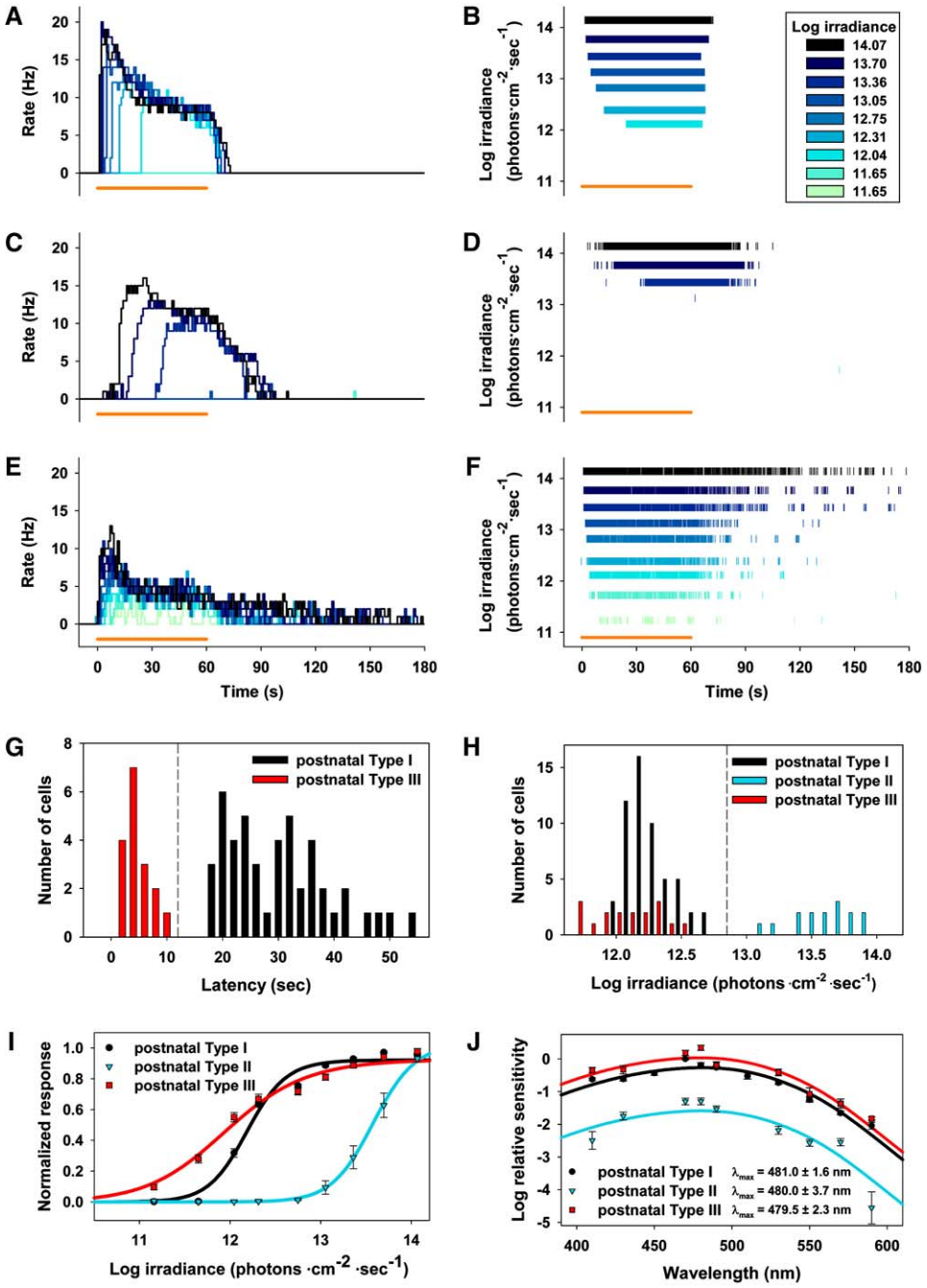

Figure 3. Postnatal ipRGCs Are Physiologically Heterogeneous

Firing rates and corresponding spike trains (A and B, respectively) for a typical postnatal type I ipRGC, type II cell (C and D), and type III cell (E and F) from the same P8 retina. Responses to increasing intensities of 480 nm light (60 s, see orange bar below figures) are shown in different colors. Spike trains (B, D, and F) are plotted on the y axis corresponding to the irradiance of the light stimulus. Light responses of single units isolated from P8 retinas (four retinas from four mice, 87 cells) were segregated into postnatal types I, II, and III by examining activity latency (G) in response to 1.10×10^{12} photons·cm^{-2}·s^{-1} 480 nm light, and photosensitivity (H) (log IR50). (I) Irradiance-response curves to 480 nm light (total number of light-induced spikes used as response parameter; n = 55, 15, and 17 for types I, II, and II, respectively; mean ± SEM). (J) Action spectra generated for each type of P8 postnatal ipRGC were fit with an opsin template (see Experimental Procedures). Action spectra for postnatal type I, II, and III ipRGCs peak at 481.0 ± 1.6 nm, 480.0 ± 3.7 nm, and 479.5 ± 2.3 nm, respectively (100, 22, and 14, type I, II, and III ipRGCs were analyzed, respectively; mean ± SEM). All experiments were performed on retinas superperfused with solutions containing glutamatergic and cholinergic inhibitors (see Experimental Procedures).

cells (Figures 4C and 4D). We segregated adult ipRGCs into adult type II and III by examining latency to activity onset in response to a subsaturating (1.13×10^{13} photons·cm^{-2}·s^{-1}, 480 nm) light pulse using the same temporal cutoff (12 s) used for categorizing postnatal ipRGCs (Figure 4E). Of the 48 adult *rd/rd* ipRGCs recorded, 32 were type II and 16 were type III. Unlike in postnatal ipRGCs, where a clear divide between type I

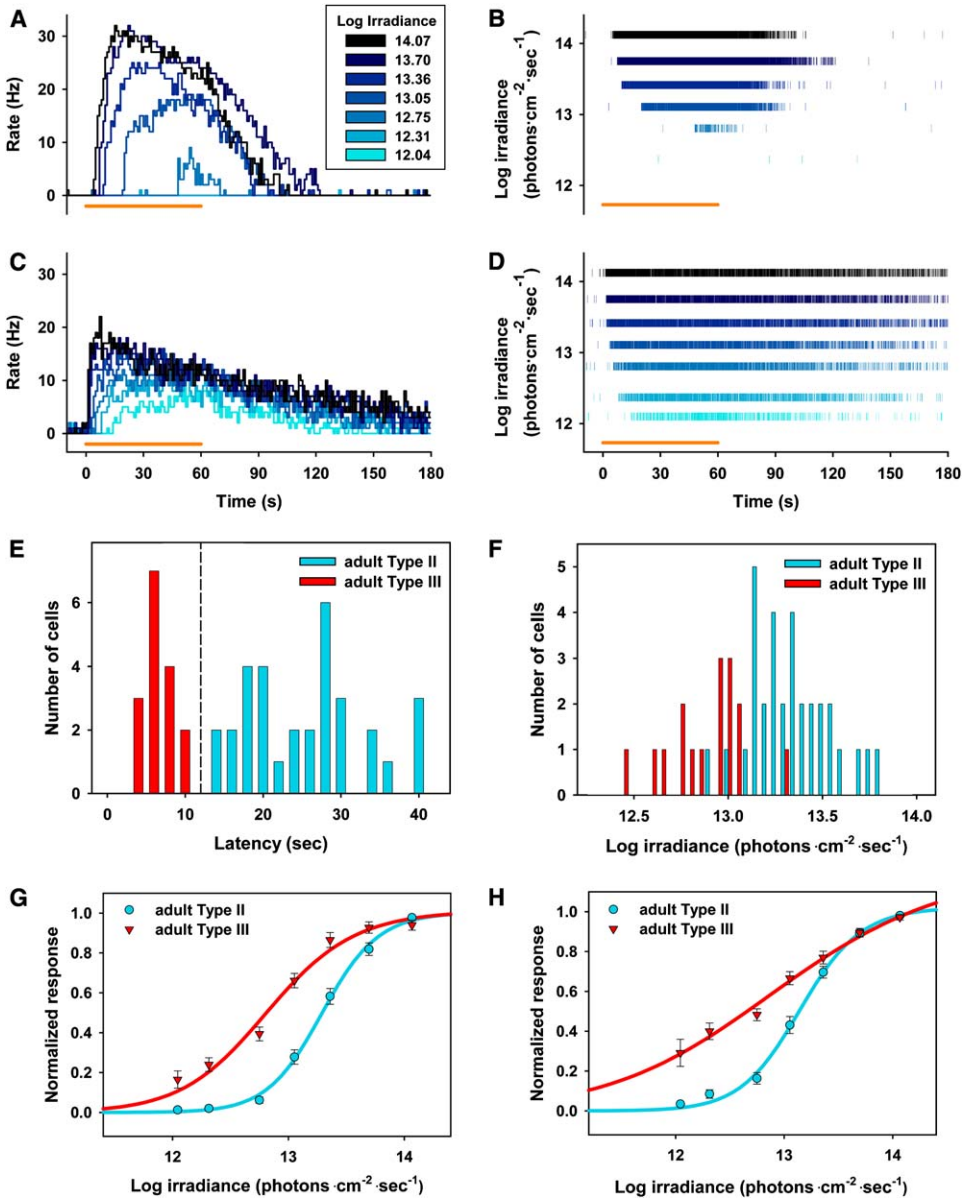

Figure 4. Adult ipRGCs Are Physiologically Heterogeneous

Firing rates and corresponding spike trains for a typical adult type II ipRGC (A and B) and adult type III cell (C and D) recorded from a 5-week-old *rd/rd* retina. Responses to increasing intensities of 480 nm light (60 s, see orange bar below figures) are shown in different colors. ipRGCs recorded from adult (5-week-old) *rd/rd* mouse retinas (four retinas from four mice, 48 cells) were segregated into adult types II and III by examining activity latency (E) in response to 1.13×10^{13} photons $\cdot$ cm$^{-2}\cdot$s^{-1} 480 nm light. (F) Distribution of photosensitivities of all cells examined (log IR50; see Experimental Procedures). Data were compiled for each cell type and used to generate irradiance-response curves to 480 nm light using total number of light-induced spikes (G) and peak firing rate (H) as response parameters (n = 32 and 16 for adult types II and III, respectively; mean ± SEM). All experiments were performed on retinas superperfused with solutions containing glutamatergic and cholinergic inhibitors (see Experimental Procedures).

and III cell types was apparent in measurements of response latency, the segregation between adult types appeared less well delineated. To confirm the presence of two discrete populations, we applied cluster analysis to sensitivity measurements of ipRGCs. Scatter plot analysis of normalized responses to different intensities of 480 nm light revealed two distinct clusters of adult responses, which agreed with the latency-based cell type segregation for 46/48 cells analyzed (Figure S4). There were no statistically significant differences in spike amplitude between adult ipRGC types (adult type II = −70.77 ± 6.38 μV; adult type III = −68.82 ± 7.78 μV).

Irradiance-response curves were generated for each of the 48 adult ipRGCs examined. Adult type II cells were approximately 10-fold less sensitive to 480 nm light than postnatal type I or III cells but exhibited photosensitivity comparable to that of postnatal type II ipRGCs (Figures 4F–4H). Adult type III cells tended to be more photosensitive than adult type II cells (Figures 4F–4H) but were not as sensitive as postnatal type III

cells. Additionally, the slopes of irradiance-response curves for adult type III cells tended to be more shallow than those of other adult ipRGCs (Figures 4G and 4H; Figure S5) and were consistent with the relatively shallow slopes of postnatal type III ipRGC irradiance-response curves (Figure S2).

Cross-Correlation Analysis of ipRGC Activity

Recent studies have shown that the number of inner retinal light-responsive cells (as assessed by calcium dye imaging) was reduced by 30%–50% after application of carbenoxolone, suggesting the presence of gap junction-mediated coupling (Sekaran et al., 2003, 2005). We applied cross-correlation analysis as a measure of neuronal coupling. We examined ipRGC activity (single units) isolated from seven P8 retinas (221 cells), four P10 retinas (156 cells), and six adult *rd/rd* retinas (84 cells). All possible pairs of ipRGCs recorded from the same retina were analyzed (Table S2). Among the 377 cells recorded from postnatal retinas, 73 cells (19.4%) showed concerted firing with other recorded cells, representing 44 pairs (the activity of some cells were correlated to more than one other cell). Of these, 12 pairs were observed on the same recording electrode, 25 were observed on linearly adjacent electrodes (200 μm spacing), five were observed on diagonally adjacent electrodes (283 μm spacing), and two pairs were seen at greater distances. Only postnatal type I cells were found to participate in concerted firing. Representative cross-correlograms (CCGs) are shown in Figure 5. Correlated pairs typically showed CCGs with a narrow trough at time zero and correlated activity on either side, consistent with direct coupling (Figure 5B, inset). The difference in timing of action potentials between correlated cells was 2.8 ± 0.5 ms in P10 retinas and 4.8 ± 0.7 ms in P8 retinas. Within correlated cell pairs, the percentage of spikes from the reference cell correlated to the activity of paired cell was 47.7% ± 2.6% for differences in spike timing of $\leq$10 ms, and 30.4% ± 2.3% for differences in spike timing of $\leq$5 ms. To ensure that cross-correlations were a measure of neuronal connectivity rather than a stimulus-induced relationship, we used shift predictor analysis (Perkel et al., 1967). Shift predictor comparison of the spikes of cell X from one trial to the timing of spikes from cell Y from multiple subsequent trials (Figure S6A) showed absence of a stimulus-induced relationship that could otherwise contribute to the central peak of the CCG. Administration of 100 μM carbenoxolone to cross-correlated pairs of cells did not eliminate correlated activity (Figures S6B and S6C), suggesting that either correlated activity was not gap junction dependent or that carbenoxolone was not effective at blocking ipRGC gap junctions. Notably, no cross-correlated cells were observed in adult *rd/rd* retinas, although this may partly be a consequence of lower numbers of cells isolated per adult retina.

Developmental Changes in ipRGC Photosensitivity

We next applied MEA recording techniques to study physiologic changes during early postnatal development. Light responses were consistently observed at P0 and P1, but photic stimulation at these ages triggered wave-like patterns of activity, precluding the extraction of single-unit spike trains (Figure S7). This suggests

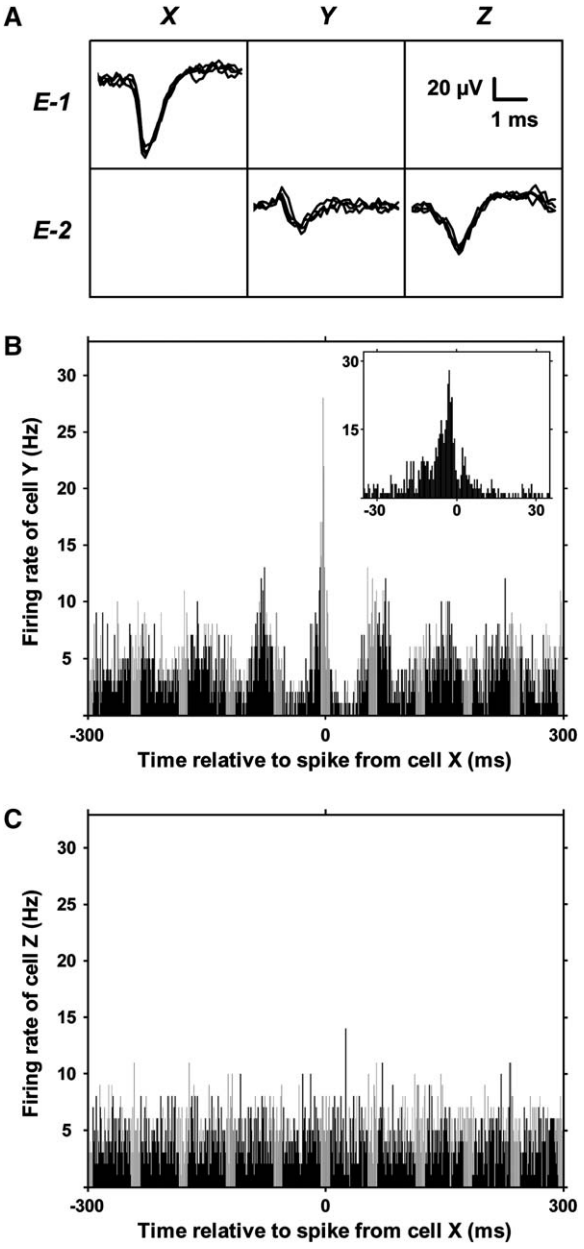

Figure 5. Correlated Activity of Inner Retinal Light Responses

Two nearby electrodes (*E-1* and *E-2*), ~280 μm apart, monitored light-induced action potentials from three cells (X, Y, and Z). (A) Spikes recorded by *E-1* (top row) and *E-2* (bottom row) have unique waveforms with different amplitudes (four representative action potentials from each cell are shown). Cross-correlograms relate the timing of action potentials from reference cell X to the action potentials from cell Y (B) and cell Z (C). Inset in (B) shows a magnification of the central peak. The timing of spikes from cell Y is correlated with that of cell X, while cells X and Z lack correlated activity. Cells X, Y, and Z represent unique units with different waveforms and with spike trains of different durations (70.7, 75.2, and 62.8 s for cells X, Y, and Z, respectively) containing different numbers of spikes (914, 752, and 703 for cells X, Y, and Z, respectively) in response to the same stimulus. P10 retina was exposed to 480 nm light (2.3×10^{13} photons·cm^{-2}·s^{-1}) while superperfused with solutions containing glutamatergic and cholinergic inhibitors (see Experimental Procedures).

that some P0–P1 ipRGCs may possess connections with other retinal neurons that allow them to initiate a wave-like activity that propagates across the retina. Perfusion

with 100 μM carbenoxolone did not eliminate P0–P1 light-induced response patterns (data not shown).

Wave-like patterns of light-induced activity are absent from ipRGCs age P2 and older, allowing reliable isolation of single-unit recordings by waveform cluster analysis. Comparison of 1 min light-induced spike trains of ipRGCs from mice ages P2–P10 revealed a significant shift in the response patterns between P4 and P6 ipRGCs (Figure 6). P2–P4 ipRGCs tended to produce spike trains of shorter duration than the 1 min light pulse, while older P6–P10 ipRGCs were capable of firing action potentials throughout the 1 min light stimulus (Figures 6A and 6B). The maximum total spike output by P2–P4 ipRGCs is significantly less than that of P6–P10 ipRGCs (data not shown). To compare the sensitivities of these cells, we normalized the irradiance-response curves of each cell to its own maximal spike output (Figure 6C), which revealed an ~10-fold increase in sensitivity to 480 nm light that occurs between P4 and P6. When a second metric—latency to peak firing rate—was used to compare P4 and P6 ipRGCs, the latter were again found to be ~10-fold more sensitive than the former (Figure 6D).

The most parsimonious explanation for the P4 to P6 transition would be that increased sensitivity of ipRGCs corresponds to increased expression of the melanopsin photopigment. Quantitative PCR was utilized to measure expression of melanopsin (*opn4*) mRNA during postnatal development (Figure 7). *opn4* mRNA is present in postnatal retinas at levels exceeding those seen in adult retina. While *opn4* rises in expression from P0 to P10, the magnitude and gradual nature of this rise does not match the abrupt >10-fold sensitivity increase observed in ipRGC photosensitivity from P4 to P6. These results suggest that changes in photosensitivity observed in postnatal ipRGC development are not solely due to changes in melanopsin transcript expression. To estimate the relative expression of melanopsin per ganglion cell, we measured the ratio of *opn4* expression to *thy1*, a ganglion cell marker (Figure 7D). The *opn4*/*thy1* ratio was consistently high in postnatal mice (compared to adult mice) at all time points sampled. Thus, it does not appear that melanopsin expression (on a per RGC basis) increases dramatically during development; rather, it shows a marked decline with adulthood. As the number of melanopsin-positive ganglion cells decreases during development (see below), it is possible that the melanopsin expression in each ipRGC is increasing during development, but we do not see changes consistent with the order of magnitude increase in sensitivity observed between P4 and P6.

To determine if morphologic changes in ipRGCs accompany the change in response characteristics observed between P4 and P6, we examined retinal cross-sections from animals sacrificed daily from P0 to P19, stained with anti-melanopsin antiserum (Provencio et al., 2002b) (Figure 8 and Figure S8). Many melanopsin-positive cells are present at P0. As noted by Sekaran et al. (2005), and consistent with our RT-PCR analysis, there is a substantial reduction in the number of melanopsin-positive cells from P0 through P19. As seen in Figure 8 and Figure S8, at ages P0–P4 melanopsin staining is seen in both the ganglion cell layer and the inner portion of the inner nuclear layer, with poorly organized

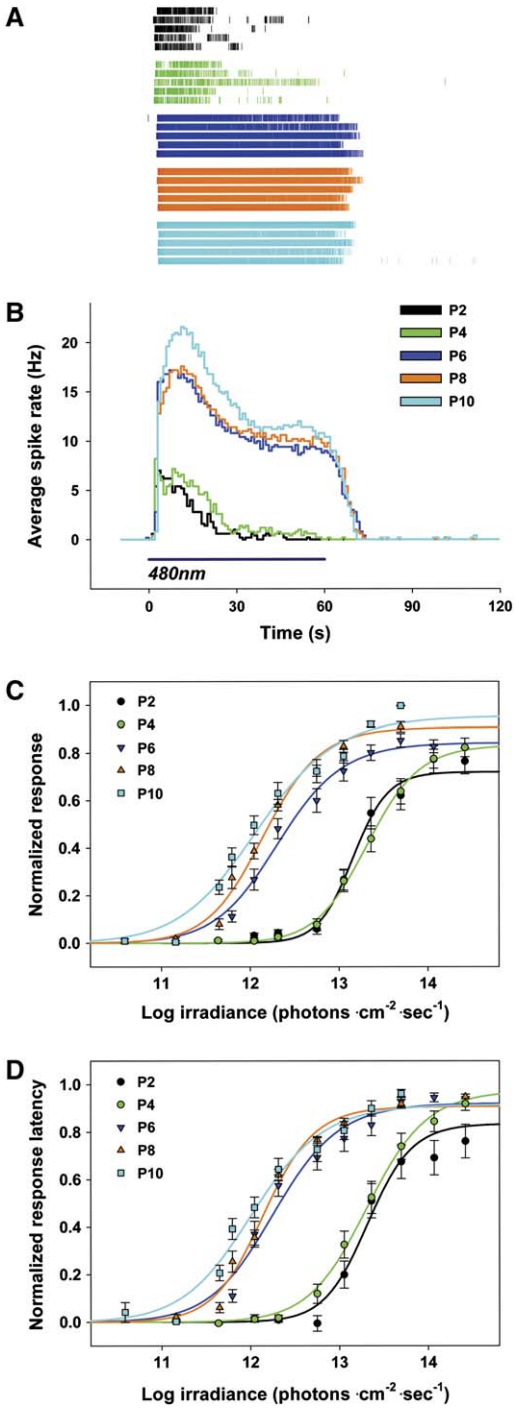

Figure 6. Developmental Changes in ipRGC Physiology

(A) Spike trains in response to saturating light stimuli for ipRGCs from wild-type mice ages P2 to P10 (480 nm, 60 s, see bar below; P2 and P4 were stimulated with 8.9×10^{14} photons·cm^{-2}·s^{-1}, and P6, P8, and P10 were stimulated with 2.04×10^{13} photons·cm^{-2}·s^{-1} to yield maximal light responses). Five representative cells are shown for each age group. (B) Average firing rates of cells shown in (A). Irradiance-response curves using total number of light-induced spikes (C) and latency to peak firing rate (D) as response parameters. Irradiance-response curves are a compilation of data from two retinas at each age ($n \geq 30$ cells; mean ± SEM). All experiments were performed on retinas superperfused with solutions containing glutamatergic and cholinergic inhibitors (see Experimental Procedures).

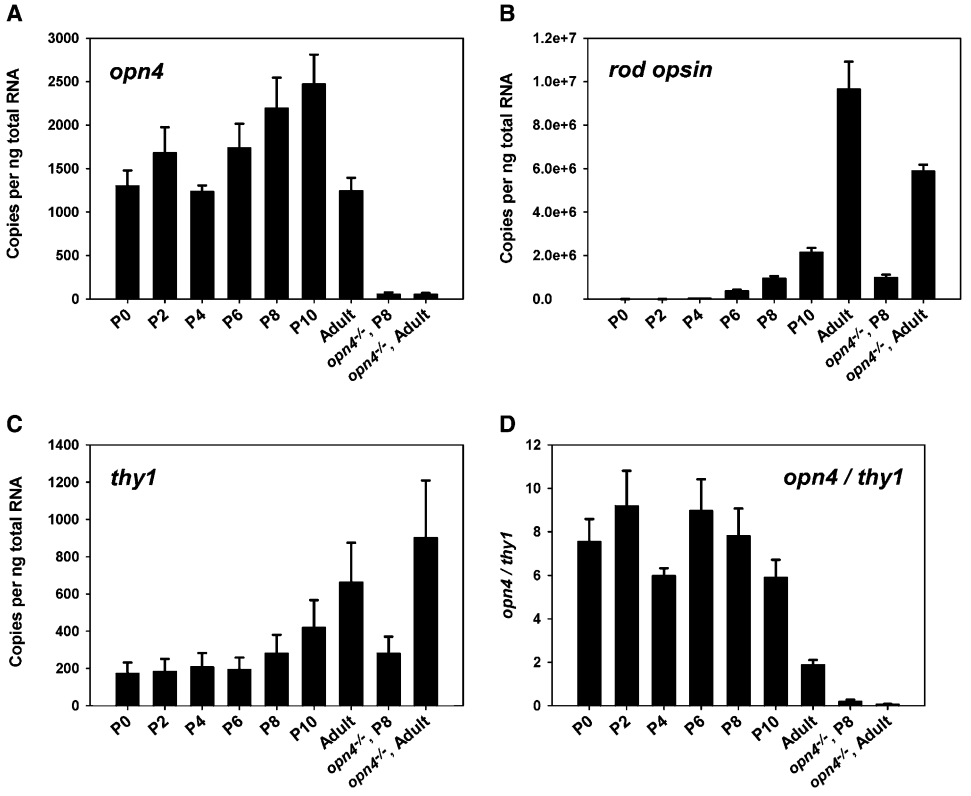

Figure 7. Melanopsin mRNA Is Expressed in Early Postnatal Retina

(A–C) Quantitative RT-PCR of total RNA derived from retinas of wild-type mice (P2, P4, P6, P8, P10, adult) and *opn4*$^{-/-}$ mice (P8, adult) examined transcript levels of *opn4* (A), *rod opsin* (B), and *thy1* (C) (n = 7; mean ± SEM).

(D) Ratio of *opn4* to *thy1*.

dendritic arborization in the inner plexiform layer. By P4, melanopsin-positive dendrites begin to separate into two distinct arbors, one in the outermost (OFF) region of the inner plexiform layer, and one in the innermost (ON) region, although at this stage there are still many dendrites between these plexuses. By P6, these two plexuses are clearly formed, although they are not as well-defined as they are in their adult forms. By P19, the pattern of expression of melanopsin cannot be distinguished from that of an adult retina, with more intense melanopsin immunoreactivity seen in outer than inner plexus.

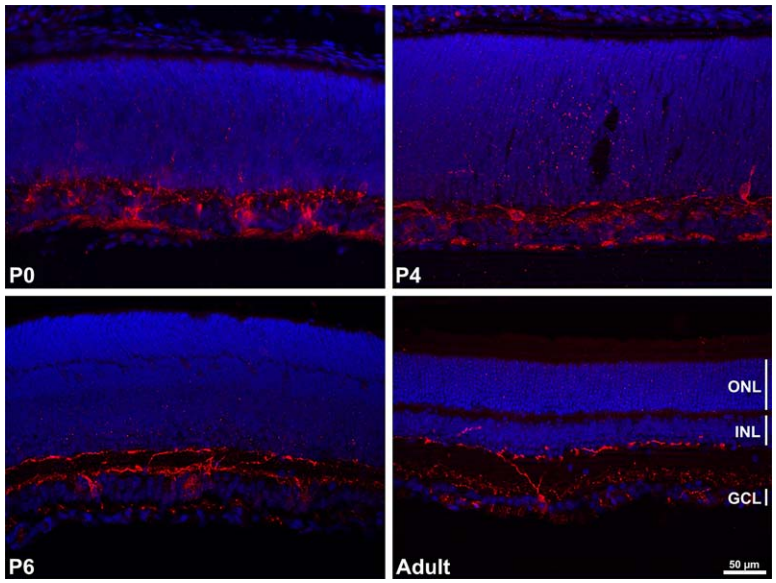

Figure 8. Developmental Timing of ipRGC Dendritic Organization

Representative immunohistochemistry demonstrating melanopsin expression (red) from mice sacrificed from P0 through adulthood (also see Figure S8). Blue indicates DAPI staining.

Discussion

We have applied the technique of MEA recording (Meister et al., 1994; Wong et al., 1993) to the study of ipRGC physiology. This technique is complementary to previously employed retrograde labeling/patch-clamp and calcium dye imaging methods (Berson et al., 2002; Dacey et al., 2005; Sekaran et al., 2003). It offers the advantages of permitting analysis of many cells simultaneously, is an extracellular recording and thus less prone to cellular rundown than patch clamping, and can be applied to animals with variable or unknown stereotactic landmarks. MEA recordings, unlike calcium dye imaging, can monitor ipRGC photoresponses without using additional light for fluorophore excitation. In theory, this technique should be applicable to the study of ipRGCs from any species, including human. Unlike retrograde labeling-based methods, however, MEA recordings cannot distinguish between ipRGCs projecting to SCN and OPN; detailed information on fine-timescale membrane potential changes are not available; and MEA does not permit analysis of the effects of membrane-impermeant drugs.

The ability to simultaneously monitor >20–30 individual ipRGCs from a single retina has revealed unexpected heterogeneity in the light-induced firing patterns of postnatal ipRGCs. Based on latency to cell firing and photosensitivity, three populations of cells were observed in P8 retina. The photoresponses of all three postnatal cell types were melanopsin dependent, had a spectral sensitivity plot that fit well with an opsin template, and had a peak spectral sensitivity near 480 nm. These findings suggest that postnatal cell types utilize the same pigment for initiation of phototransduction. Interestingly, compared to other postnatal ipRGCs, postnatal type III cells tend to have shallow irradiance-response curves. Indeed, for certain response parameters (such as total light-induced spikes and peak firing rate), postnatal type III cells have irradiance-response curves that are almost linear over a 1000-fold range of irradiances. This type of response could serve as an accurate "light meter" over a broad dynamic range. A similar linear relationship between irradiance and total light-induced spikes was noted in ipRGCs identified by retrograde labeling from the OPN in macaque monkeys (Dacey et al., 2005) but has not been previously appreciated in recordings from mouse ipRGCs.

While our data support the identification of three discrete ipRGC response types during murine postnatal development, we do not know whether these have functional significance during development. Alternatively, the subtypes could constitute an epiphenomenon arising from dynamic developmental changes. During the P8–P10 period, the retina and ipRGCs are undergoing significant anatomical and cell number changes. With our current MEA recording technique, we are not able to correlate the anatomical or apoptotic state of individual cells with their physiologic recordings. It is possible that one or more of the postnatal ipRGC functional types arise from cells at specific transient developmental stages or from cells undergoing programmed cell death.

However, we also observed substantial functional diversity in ipRGCs recorded from adult *rd/rd* retinas. These cells displayed patterns of activity with characteristics that were similar to those of postnatal type II and type III cells, although adult ipRGCs tended to be less sensitive than postnatal type I or III cells. Similar to postnatal type III cells, adult type III ipRGCs tended to have irradiance-response curves that were more shallow than other ipRGCs. Given the relative preponderance of postnatal type I cells and adult type II cells, it is possible that the postnatal type I cells mature into adult type II cells; however, we cannot exclude the possibility that postnatal type I cells may preferentially undergo apoptosis, perhaps accounting for the ~4-fold decrease in melanopsin-positive cell number from birth to adulthood (Sekaran et al., 2005). The mechanisms underlying other developmental changes between postnatal and adult cells also need to be elucidated: specifically, the mechanisms underlying the low spike amplitudes of postnatal type III cells, and the differences in photosensitivity between postnatal and adult type III cells are unknown. Definitively linking postnatal P8 and adult cell types will require analysis of ipRGCs from retinas harvested from intermediate time points.

The functional significance of the different ipRGC firing patterns and sensitivities is presently not known. It is possible that different ipRGC cell types project to different brain regions; this may explain the relative uniformity of electrophysiological responses seen in patch-clamp studies of cells retrograde-labeled from the SCN (Berson et al., 2002). Alternatively, a range of physiologic responses may expand the overall sensitivity and kinetics of nonvisual photoreception to each nonvisual target region. It is possible that these different patterns of ipRGC activity could serve to encode different elements of irradiance information (i.e., integration of irradiance over time or temporal changes in irradiance).

Interestingly, at least two morphologic types of ipRGCs have been observed in adult mice: ipRGCs with dendritic processes primarily in the inner regions of the inner plexiform layer (typically considered part of the ON pathway) and ipRGCs with dendrites primarily in outer regions of the inner plexiform layer (typically considered part of the OFF pathway). (Provencio et al., 2002a). Technical limitations of our present technique—principally the difficulty in anatomically identifying the cells being recorded on the MEA—prevent evaluation of potential relationships between morphologic and physiologic subtypes of ipRGCs. While the current study has demonstrated specific physiologic types of ipRGC responses, additional experiments comparing the physiology of individual ipRGCs with their respective dendritic arborizations, receptive fields, and central projections will be needed to fully describe and classify both postnatal and adult ipRGCs cell types.

Sekaran et al. (2003, 2005) in their calcium dye imaging studies of ipRGCs also suggested the presence of different subtypes of cells. The three cell types were respectively characterized by sustained, transient, and repetitive calcium flux in response to light stimuli. In contrast, electrophysiologically, most ipRGCs showed sustained firing by P6, with P8 and adult cells showing persistent firing for several seconds after lights off. Of note, the irradiances necessary to observe ipRGC activity by Ca^{2+} dye imaging were substantially greater (>10-fold) than that necessary in the present study to observe cell firing activity and also greater than irradiances necessary to elicit ipRGC-dependent behavioral

responses in vivo (Panda et al., 2003). It is possible that the three subtypes identified by Sekaran et al. represent the behavior of the cell types described in the present study in response to very high irradiance.

Ca^{2+} dye imaging studies have also suggested the presence of coupling between ipRGCs and themselves or other cells (Sekaran et al., 2003, 2005). Sekaran et al. noted that application of carbenoxolone (a putative gap junction blocker) at 100 μM for adult *rd/rd cl* retinas and 10 μM for early postnatal retinas decreased the number of light-responsive cells detected by 50% and 33%–44% in adult and early postnatal retinas, respectively. By using MEA recordings to examine many ipRGCs from the same retina simultaneously, we observed highly correlated firing occurring in ~20% of single units isolated from P8–10 retinas. The width and offset of the central peak of CCGs (Table S2) were consistent with reports of gap junctional coupling of retinal ganglion cells (Hu and Bloomfield, 2003). We did not detect concerted activity among the ipRGCs recorded from adult *rd/rd* retinas, although this survey was partially biased due to the lower number of ipRGCs isolated per adult retina. While carbenoxolone treatment abrogated apparent cell-cell coupling of Ca^{2+} release (Sekaran et al., 2003), carbenoxolone did not eliminate synchronous activity between light-responsive cells detected by MEA recordings. The reason for this discrepancy is unclear. However, it is worth noting that carbenoxolone has nonspecific effects, including inhibition of voltage-gated calcium channels (Vessey et al., 2004), and may influence neuronal properties such as action potential threshold and firing rate (Rouach et al., 2003). We observed nonspecific effects of carbenoxolone soon after application, including subtle changes in action potential waveforms (data not shown).

Use of MEA recordings has also allowed us to characterize the development of ipRGC photosensitivity. Previous studies have demonstrated light-induced c-*fos* expression in melanopsin-positive cells from birth onward, demonstrating photoreceptive activity in very young animals (Hannibal and Fahrenkrug, 2004). Munoz Llamosas et al. (2000) could not detect c-*fos* expression in the recipient murine SCN until P4. In mouse, Weaver and Reppert (1995), Hannibal and Fahrenkrug (2004), and Sekaran et al. (2005) observed photic induction of c-*fos* mRNA in response to light from P0, but with much reduced amplitudes compared with P4 or older animals; similar weak photic SCN c-*fos* induction has been observed in P1 rats (Leard et al., 1994). Sekaran et al. (2005) have recently demonstrated that robust Ca^{2+} release can be seen from ipRGCs as early as P0, and that melanopsin-expressing cells have made projections to the SCN by this time. Taken together, these results might suggest that ipRGCs have reduced firing of action potentials in response to light prior to P4; alternatively, the absence of c-*fos* expression in the SCN might indicate immaturity of the retinohypothalamic tract or of c-*fos* induction mechanisms in the SCN. Our results suggest that ipRGCs are capable of firing action potentials from birth and show discernible spike trains by P2, but that most ipRGCs do not develop mature, sustained levels of firing in response to minute-long light pulses until after P4. Additionally, P2–P4 ipRGCs are relatively insensitive to light compared to P6 and older postnatal ipRGCs. Thus, changes in the firing patterns and photosensitivity of ipRGCs during development may explain the weak induction of c-*fos* in the SCN prior to P4 and strong induction after P6 seen in previous studies. Interestingly, this P4 to P6 transition period coincides with the dendritic organization of melanopsin-expressing cells to inner and outer regions of the inner plexiform layer. It is unclear whether this morphologic transition influences maturation of ipRGC photosensitivity and firing patterns. Since melanopsin appears to be highly expressed throughout early development, the sustained light response of ipRGCs in older animals is likely not due to a change in an intrinsic property of melanopsin, but rather a maturation of additional signaling components. The identities of these components remain to be determined.

Experimental Procedures

Animals and MEA Recording Conditions

All experiments were performed in accordance with Association for Research in Vision and Ophthalmology guidelines for animal studies, and under approved animal studies protocol. Mice were maintained in LD 12:12. *opn4*$^{-/-}$ were graciously provided by Drs. John Hogenesch and Satchidananda Panda and maintained as homozygotes. Adult *rd/rd* mice (5 weeks old) were in the C3H background. C57Bl/6 mice were used as wild-type strain.

Mice were sacrificed by CO_2 narcosis and cervical dislocation. Isolated mouse retina was positioned with the vitreal face in contact with a planar array of 60 electrodes (Multi Channel Systems) and superperfused (1 ml/min) with a bicarbonate-buffered physiologic solution (125 mM NaCl, 2.5 mM KCl, 1 mM $MgCl_2$, 1.25 mM NaH_2PO_4, 20 mM glucose, 26 mM $NaHCO_3$, 2 mM $CaCl_2$, 500 μM glutamine) oxygenated with 95% O_2/5% CO_2. The temperatures of both perfusate and tissue chamber were maintained at 30.8°C. High-potassium solution (50 mM) was made by substituting equimolar KCl for NaCl.

MEA Recordings

Electrophysiologic recordings were performed using planar arrays with 60 electrodes (30 μm diameter, 200 μm interelectrode spacing; Multi Channel Systems). Raw electrical signals were amplified, filtered, digitized through an A/D card (National Instruments), and written to disk as described previously (Holy et al., 2000). Custom software was used to acquire these data and perform offline analysis (Holy et al., 2000). Single units (with distinct interspike refractory periods) were isolated via cluster analysis based on differences in spike waveform.

Pharmacology

Although young postnatal mice lack functional input from rod and cone photoreceptors to retinal ganglion cells, the inner retinal neurons of these young animals participate in waves of spontaneous activity (Wong et al., 1993). Pharmacologic blockade of spontaneous developmental waves has been previously described (Wong et al., 2000). To inhibit spontaneous retinal waves (as well as any potential input from rod and cone photoreceptors), postnatal mouse retinas were recorded in physiologic solution containing glutamatergic [50 μM d(−)-2-amino-5-phosphonopentanoic acid (d-APV); 10 μM CNQX] and cholinergic (5 nM epibatidine) inhibitors. For adult *rd/rd* retinal recordings, this cocktail was sufficient to block any potential signaling from outer retinal photoreceptors. Carbenoxolone was used at 100 μM. All drugs were purchased from Sigma Aldrich (St. Louis, MO).

Light Stimuli

After dark adaptation in a light-tight enclosure, retinas were stimulated with a Xenon light source (Sutter Instruments) fed through a liquid light guide and diffusing filter (Thorlabs, Inc.). Intensity and wavelength of lights were adjusted via neutral density and narrow band-pass interference filters (Thorlabs, Inc.) and calibrated using a radiometer (Advanced Photonics International). Light stimuli were delivered and monitored using a computer-controlled shutter (Vincent Associates).

Light Responsiveness, Irradiance-Response Relations, and Action Spectra

To test for light-responsive inner retinal activity in *wild-type* and *opn4*$^{-/-}$ mice, retinas were exposed to 3 × 1 min pulses of light (480 nm, 60 s, 5.0 × 10^{13} photons·cm^{-2}·s^{-1}) separated by 3 min darkness. All action potentials recorded from MEA electrodes were used for these analyses without spike sorting to isolate single units. Electrodes that recorded more than twice as many spikes during each light pulse as during the preceding 1 min of darkness, for all three stimulations, were taken as light responsive. Likewise, electrodes that recorded twice as many spikes during KCl application as before stimulation were taken as KCl responsive. Light-responsive electrodes typically showed ~900 times more spikes in the light period as in the dark. The results of these experiments were confirmed using the same protocol at additional light intensities (2.3 × 10^{13} photons·cm^{-2}·s^{-1}, 1.1 × 10^{13} photons·cm^{-2}·s^{-1}).

Irradiance-response curves were generated by plotting normalized response as a function of log irradiance (photons·cm^{-2}·s^{-1}). The normalized response of an individual cell to a specific light stimulus was calculated as a fraction of its maximal response to 480 nm light. Each response parameter was analyzed separately. The response parameters used were (1) total number of light-induced spikes; (2) steady-state activity, assessed by counting the number of spikes during the last 15 s of a 60 s light pulse; (3) peak firing rate, calculated using a moving average; and (4) latency to peak firing rate in response to a 60 s light pulse, calculated as the time gap between onset of the stimulus and the time of peak firing rate calculated using a moving average. For irradiance-response relations, latency measurements were normalized such that the shortest latency = maximal response. Normalized data for each parameter were fit with a Michaelis-Menten equation (Baylor et al., 1974; Dacey et al., 2005; Naka and Rushton, 1966), and log irradiance values that generate half-maximal response (log IR50) were recorded as a measure of photosensitivity (Sigmaplot). To generate action spectra, we examined ipRGC responses to different wavelengths of light. The order of exposure to different wavelengths of light was randomized to avoid potential influences of a bistable photopigment. All cells were tested with 480 nm light to control for photosensitivity at this wavelength. Data from ipRGC types I, II, and III were compiled, and irradiance-response curves were generated for each cell type. Relative sensitivity was calculated as $\log_{10}(IR50_{max}/IR50)$, where $IR50_{max}$ = IR50 at the wavelength of maximum sensitivity of postnatal type I cells. Log relative sensitivities of ipRGCs to each wavelength tested were fit with an opsin template using Lamb's equation with an additional constant to allow the relative sensitivities of the three spectra to vary relative to one another (Lamb, 1995). For each cell type, action spectra constructed using the four response parameters described above were found to be in tight agreement; an average of these spectra is presented.

Clustering of Adult Cell Types

Normalized responses of adult ipRGCs (described in Figure 4) to 480 nm light at two different intensities (2.06 × 10^{12} and 5.61 × 10^{12} photons·cm^{-2}·s^{-1}), using total light-induced spikes as the response parameter, were utilized. The probability density of the data points in this two-dimensional space was constructed by an adaptive kernel density method, convolving each data point with an Epanechnikov kernel (inverted parabola, cut off at zero) of radius *R* equal to the distance to its tenth nearest neighbor. Points were then flowed uphill to local maxima in probability density; once convergence was achieved, modes within the median *R* were lumped together (Fukunaga and Hostetler, 1975; Silverman, 1986).

Cross-Correlation Analysis

CCGs were constructed to test for synchronous neuronal activity. The timing of one cell's activity relative to that of a reference cell was plotted as a histogram using 0.5 ms bins over a window of 0.5 s around the reference cell's spike times (time zero). The central peak of the CCG was fit with a Gaussian curve, and the width was calculated as previously described by Brivanlou et al. (1998). The maximum of this Gaussian fit was considered the difference in timing between correlated cells. Confidence limits (95% and 99%) were calculated based on the Poisson equation if the expected firing rate (counts per bin) was less than 30 or on a Gaussian approximation if this number was greater than or equal to 30 (Abeles, 1982). Shift predictor was utilized to test for potential correlations due to costimulation-induced firing rate increases (Perkel et al., 1967). Shift predictor analysis calculates a new CCG by comparing a reference cell's activity in an individual trial to the spike trains of a different cell from time-shifted trials (subsequent or prior trials); correlations induced by the stimulus would be expected to survive this procedure, as the stimulus was identical across trials, but correlations arising from fluctuations in neural activity are removed. Multiple trials were utilized to compute an average shift predictor. Our data produced flat shift predictor histograms, suggesting a neural origin for these cross-correlations.

Immunocytochemistry

Starting at the day of birth (P0), eyes were removed from C57Bl/6J mice on each successive day of development. The anterior pole and lens were removed from postnatal eyes when possible. Eyes were fixed overnight in 4% paraformaldehyde in 1× PBS, transferred to 30% sucrose for several hours, and embedded in TissueTek before being cryosectioned at 16 μm. Sections were affixed to poly-L-lysine-coated slides and refrigerated at −80ºC until processing. Slides were thawed briefly in PBS at 4ºC, incubated for 30 min in a blocking solution of 1.5% goat serum, and then rinsed in PBS. The slides were incubated overnight in 300 μl per slide of an incubating buffer (0.25% carrageenan-λ and 1.0% BSA, and 3.0% Triton X-100 in TBS) containing a 1:2500 dilution of rabbit anti-melanopsin antiserum raised against the 15 N-terminal amino acids of mouse melanopsin as predicted by the published gene sequence (Provencio et al., 2002b). Subsequently, slides were rinsed in PBS, and 300 μl of a 1:500 dilution of Cy3-conjugated anti-rabbit IgG secondary antibody in incubating buffer was placed on each slide. Finally, slides were incubated at room temperature for an hour, rinsed in PBS, and mounted in aqueous mounting medium containing DAPI (nuclear stain) before examination via fluorescence microscopy.

Quantitative PCR

Total RNA isolated from retinal tissue (Qiagen) was treated with DNase to remove genomic DNA (Ambion). Reverse transcription of total RNA was performed using MuLV reverse transcriptase with oligo $d(T)_{16}$ primer (Applied Biosystems); resulting cDNA products were amplified in quantitative PCR reactions using IQ Sybr green super mix (Bio-Rad). β-*actin*, *thy1*, and *rod opsin* primer sequences were used from Peirson et al. (2004). *opn4* primers were designed to target exonic regions spanning the first putative intron of *opn4*. Forward primer: 5′-TTTCCATGGCCTTAGCTCCTCTGA-3′. Reverse primer: 5′-TGTAGATGACCGTCAGATTGCCCA-3′. Differences in RNA loading between samples were normalized using the level of β-actin expression. Melt curves showed amplification of single products in all cases.

Supplemental Data

The Supplemental Data include eight supplemental figures and two supplemental tables and can be found with this article online at http://www.neuron.org/cgi/content/full/48/6/987/DC1/.

Acknowledgments

We thank J. Guo and R. Hendrickson for assistance with MEA analysis software; P.D. Lukasiewicz, B.T. Sagdullaev, R.O. Wong, E.D. Eggers, and J. de Brecht for aid with electrophysiology and pharmacology; L.A. Owens for animal care; G. Gusdorf for MEA hardware assistance; and M.A. Brantley for space support. D.C.T. was supported by NIH training grant T32 EY13360. D.C.T. and D.Z. were supported by the Medical Scientist Training Program of Washington University Medical School. R.N.V.G. was supported by the Culpeper Physician-Scientist Award of the Rockefeller Brothers Foundation, a grant from the McDonnell Foundation for Systems Neuroscience, and NIH R01-EY14988.

Received: May 9, 2005
Revised: July 28, 2005
Accepted: September 22, 2005
Published: December 21, 2005

References

Abeles, M. (1982). Quantification, smoothing, and confidence limits for single-units' histograms. J. Neurosci. Methods *5*, 317–325.

Bakall, B., Marmorstein, L.Y., Hoppe, G., Peachey, N.S., Wadelius, C., and Marmorstein, A.D. (2003). Expression and localization of bestrophin during normal mouse development. Invest. Ophthalmol. Vis. Sci. *44*, 3622–3628.

Baylor, D.A., Hodgkin, A.L., and Lamb, T.D. (1974). The electrical response of turtle cones to flashes and steps of light. J. Physiol. *242*, 685–727.

Berson, D.M., Dunn, F.A., and Takao, M. (2002). Phototransduction by retinal ganglion cells that set the circadian clock. Science *295*, 1070–1073.

Brivanlou, I.H., Warland, D.K., and Meister, M. (1998). Mechanisms of concerted firing among retinal ganglion cells. Neuron *20*, 527–539.

Dacey, D.M., Liao, H.W., Peterson, B.B., Robinson, F.R., Smith, V.C., Pokorny, J., Yau, K.W., and Gamlin, P.D. (2005). Melanopsin-expressing ganglion cells in primate retina signal colour and irradiance and project to the LGN. Nature *433*, 749–754.

Fahrenkrug, J., Nielsen, H.S., and Hannibal, J. (2004). Expression of melanopsin during development of the rat retina. Neuroreport *15*, 781–784.

Foster, R.G., Provencio, I., Hudson, D., Fiske, S., De Grip, W., and Menaker, M. (1991). Circadian photoreception in the retinally degenerate mouse (*rd/rd*). J. Comp. Physiol. [A] *169*, 39–50.

Freedman, M.S., Lucas, R.J., Soni, B., von Schantz, M., Munoz, M., David-Gray, Z., and Foster, R. (1999). Regulation of mammalian circadian behavior by non-rod, non-cone, ocular photoreceptors. Science *284*, 502–504.

Fukunaga, K., and Hostetler, L. (1975). The estimation of the gradient of a density function, with applications in pattern recognition. IEEE Trans. Info. Thy. *21*, 32–40.

Hannibal, J., and Fahrenkrug, J. (2004). Melanopsin containing retinal ganglion cells are light responsive from birth. Neuroreport *15*, 2317–2320.

Hannibal, J., Hindersson, P., Knudsen, S.M., Georg, B., and Fahrenkrug, J. (2002). The photopigment melanopsin is exclusively present in pituitary adenylate cyclase-activating polypeptide-containing retinal ganglion cells of the retinohypothalamic tract. J. Neurosci. *22*, RC191.

Hattar, S., Liao, H.W., Takao, M., Berson, D.M., and Yau, K.W. (2002). Melanopsin-containing retinal ganglion cells: architecture, projections, and intrinsic photosensitivity. Science *295*, 1065–1070.

Hattar, S., Lucas, R.J., Mrosovsky, N., Thompson, S., Douglas, R.H., Hankins, M.W., Lem, J., Biel, M., Hofmann, F., Foster, R.G., and Yau, K.W. (2003). Melanopsin and rod-cone photoreceptive systems account for all major accessory visual functions in mice. Nature *424*, 75–81.

Holy, T.E., Dulac, C., and Meister, M. (2000). Responses of vomeronasal neurons to natural stimuli. Science *289*, 1569–1572.

Hu, E.H., and Bloomfield, S.A. (2003). Gap junctional coupling underlies the short-latency spike synchrony of retinal alpha ganglion cells. J. Neurosci. *23*, 6768–6777.

Lamb, T.D. (1995). Photoreceptor spectral sensitivities: common shape in the long-wavelength region. Vision Res. *35*, 3083–3091.

Leard, L.E., Macdonald, E.S., Heller, H.C., and Kilduff, T.S. (1994). Ontogeny of photic-induced c-fos mRNA expression in rat suprachiasmatic nuclei. Neuroreport *5*, 2683–2687.

Lucas, R.J., Freedman, M.S., Munoz, M., Garcia-Fernandez, J.M., and Foster, R.G. (1999). Regulation of the mammalian pineal by non-rod, non-cone, ocular photoreceptors. Science *284*, 505–507.

Lucas, R.J., Douglas, R.H., and Foster, R.G. (2001). Characterization of an ocular photopigment capable of driving pupillary constriction in mice. Nat. Neurosci. *4*, 621–626.

Lucas, R.J., Hattar, S., Takao, M., Berson, D.M., Foster, R.G., and Yau, K.W. (2003). Diminished pupillary light reflex at high irradiances in melanopsin-knockout mice. Science *299*, 245–247.

Meister, M., Pine, J., and Baylor, D.A. (1994). Multi-neuronal signals from the retina: acquisition and analysis. J. Neurosci. Methods *51*, 95–106.

Melyan, Z., Tarttelin, E.E., Bellingham, J., Lucas, R.J., and Hankins, M.W. (2005). Addition of human melanopsin renders mammalian cells photoresponsive. Nature *433*, 741–745.

Munoz Llamosas, M., Huerta, J.J., Cernuda-Cernuda, R., and Garcia-Fernandez, J.M. (2000). Ontogeny of a photic response in the retina and suprachiasmatic nucleus in the mouse. Brain Res. Dev. Brain Res. *120*, 1–6.

Naka, K.I., and Rushton, W.A.H. (1966). S-potentials from luminosity units in the retina of fish (Cyprinidae). J. Physiol. *185*, 587–599.

Newman, L.A., Walker, M.T., Brown, R.L., Cronin, T.W., and Robinson, P.R. (2003). Melanopsin forms a functional short-wavelength photopigment. Biochemistry (Mosc.) *42*, 12734–12738.

Panda, S., Provencio, I., Tu, D.C., Pires, S.S., Rollag, M.D., Castrucci, A.M., Pletcher, M.T., Sato, T.K., Wiltshire, T., Andahazy, M., et al. (2003). Melanopsin is required for non-image-forming photic responses in blind mice. Science *301*, 525–527.

Panda, S., Nayak, S.K., Campo, B., Walker, J.R., Hogenesch, J.B., and Jegla, T. (2005). Illumination of the melanopsin signaling pathway. Science *307*, 600–604.

Peirson, S.N., Bovee-Geurts, P.H., Lupi, D., Jeffery, G., DeGrip, W.J., and Foster, R.G. (2004). Expression of the candidate circadian photopigment melanopsin (*Opn4*) in the mouse retinal pigment epithelium. Brain Res. Mol. Brain Res. *123*, 132–135.

Perkel, D.H., Gerstein, G.L., and Moore, G.P. (1967). Neuronal spike trains and stochastic point processes. II. Simultaneous spike trains. Biophys. J. *7*, 419–440.

Provencio, I., Jiang, G., De Grip, W.J., Hayes, W.P., and Rollag, M.D. (1998). Melanopsin: An opsin in melanophores, brain, and eye. Proc. Natl. Acad. Sci. USA *95*, 340–345.

Provencio, I., Rodriguez, I.R., Jiang, G., Hayes, W.P., Moreira, E.F., and Rollag, M.D. (2000). A novel human opsin in the inner retina. J. Neurosci. *20*, 600–605.

Provencio, I., Berson, D.M., Richardson, R.C., Rollag, M.D., and Castrucci, A.M. (2002a). Melanopsin immunoreactivity in retinal ganglion cells. Paper presented at: Association for Research in Vision and Ophthalmology (Fort Lauderdale, Florida).

Provencio, I., Rollag, M.D., and Castrucci, A.M. (2002b). Photoreceptive net in the mammalian retina. Nature *415*, 493.

Qiu, X., Kumbalasiri, T., Carlson, S.M., Wong, K.Y., Krishna, V., Provencio, I., and Berson, D.M. (2005). Induction of photosensitivity by heterologous expression of melanopsin. Nature *433*, 745–749.

Ratto, G.M., Robinson, D.W., Yan, B., and McNaughton, P.A. (1991). Development of the light response in neonatal mammalian rods. Nature *351*, 654–657.

Rouach, N., Segal, M., Koulakoff, A., Giaume, C., and Avignone, E. (2003). Carbenoxolone blockade of neuronal network activity in culture is not mediated by an action on gap junctions. J. Physiol. *553*, 729–745.

Sekaran, S., Foster, R.G., Lucas, R.J., and Hankins, M.W. (2003). Calcium imaging reveals a network of intrinsically light-sensitive inner-retinal neurons. Curr. Biol. *13*, 1290–1298.

Sekaran, S., Lupi, D., Jones, S.L., Sheely, C.J., Hattar, S., Yau, K.W., Lucas, R.J., Foster, R.G., and Hankins, M.W. (2005). Melanopsin-dependent photoreception provides earliest light detection in the mammalian retina. Curr. Biol. *15*, 1099–1107.

Silverman, B.W. (1986). Density Estimation for Statistics and Data Analysis (Boca Raton, FL: Chapman & Hall).

Van Gelder, R.N., Wee, R., Lee, J.A., and Tu, D.C. (2003). Reduced pupillary light responses in mice lacking cryptochromes. Science *299*, 222.

Vessey, J.P., Lalonde, M.R., Mizan, H.A., Welch, N.C., Kelly, M.E., and Barnes, S. (2004). Carbenoxolone inhibition of voltage-gated Ca channels and synaptic transmission in the retina. J. Neurophysiol. *92*, 1252–1256.

Weaver, D.R., and Reppert, S.M. (1995). Definition of the developmental transition from dopaminergic to photic regulation of c-fos

gene expression in the rat suprachiasmatic nucleus. Brain Res. Mol. Brain Res. *33*, 136–148.

Wong, R.O., Meister, M., and Shatz, C.J. (1993). Transient period of correlated bursting activity during development of the mammalian retina. Neuron *11*, 923–938.

Wong, W.T., Myhr, K.L., Miller, E.D., and Wong, R.O. (2000). Developmental changes in the neurotransmitter regulation of correlated spontaneous retinal activity. J. Neurosci. *20*, 351–360.